Contents lists available at ScienceDirect

Transactions of Nonferrous Metals Society of China

36(2026) 416−432

www.tnmsc.cn

Ce-adipate as green corrosion inhibitor of AA7075 alloy

Jovanka N. PEJIĆ [a], Dunja D. MARUNKIĆ [a], Bojana M. RADOJKOVIĆ [a,*], Bore V. JEGDIĆ [a], Sanja G. ERAKOVIĆ PANTOVIĆ [a], Anđela R. SIMOVIĆ [a], Behar ALIĆ [b], Milica GVOZDENOVIĆ [c]

[a] Institute of Chemistry, Technology, and Metallurgy, University of Belgrade, Njegoševa 12, Belgrade, Serbia;
[b] Metallurgical Institute "Kemal Kapetanović", Travnička cesta 7, 72000 Zenica, Bosnia and Herzegovina;
[c] Faculty for Technology and Metallurgy, University of Belgrade, Karnegijeva 4, Belgrade, Serbia

Abstract: The effect of low concentrated green inhibitors based on Ce-adipate and Ce-chloride on the corrosion of 7075 aluminum alloy in neutral NaCl electrolyte was studied. Corrosion studies were carried out using electrochemical impedance spectroscopy (EIS) and linear sweep voltammetry (LSV) while scanning electron microscopy (SEM) and X-ray photoelectron spectroscopy (XPS) were used to conduct surface studies of the alloy upon immersion in the corrosion media. The electrochemical experiments reveal a better inhibitory effect of Ce-adipate than Ce-chloride owing to a higher polarization resistance value (about two times), and a lower corrosion current density. However, both inhibitors act as cathodic inhibitors, show high resistance to pitting corrosion, and enable sufficient protection during prolonged immersion (240 h) in corrosion media. The XPS analysis confirms the presence of cerium in the oxidation states of Ce(III) and Ce(IV) together with the carboxylate —COO^- groups and C—C and C—H bonds on the tested specimen with Ce-adipate inhibitor, which are connected to the increased anti-corrosion efficiency.
Keywords: AA7075; green corrosion inhibitors; Ce-adipate

1 Introduction

The AA7075 belongs to the group of aluminum alloys with maximum strength. These alloys are used in various industries, such as aviation. The specific strength for this alloy is several times higher than for carbon steel [1−3]. One of the major disadvantages of these alloys is the susceptibility to localized types of corrosion in environments containing chloride ions [1].

AA7075 is applied after one-step aging (T6) or after two-step aging (T76 and T73). The T76 and T73 aged alloy has a higher resistance to exfoliation corrosion and stress corrosion cracking, but to some extent has lower strength.

Besides strengthening precipitates (GP zones, η', and η phases) with nanometer dimensions, in AA7075 microstructure, cathodic intermetallic compounds are present, for instance, Al_3Fe, $(Al,Cu)_6(Fe,Cu)$, and Al_7Cu_2Fe, as well as anodic Mg_2Si intermetallic compounds (IMCs) all with micrometer dimensions [4−6]. The corrosion behaviour of AA7075 is very complex due to the presence of different electronegativity of IMCs. As a consequence, these alloys after one-step and after two-step aging are prone to general and pitting corrosion [3]. Accordingly, the development of methods for increasing the corrosion resistance of the AA7075 is of great importance. The use of corrosion inhibitors can be an effective method of corrosion protection of these and other aluminum alloys.

Hexavalent chromium compounds (chromates) have been widely used as effective inhibitors for the corrosion protection of aluminum alloys and many

Corresponding author: *Bojana M. RADOJKOVIĆ, E-mail: bojana.radojkovic@ihtm.bg.ac.rs
https://doi.org/10.1016/S1003-6326(25)66973-1
Received 22 May 2024; accepted 19 December 2024

metals [7]. However, because of the high toxicity and carcinogenicity of the Cr(VI) compounds, there was a need to find environmentally acceptable corrosion inhibitors with satisfying protective ability. In the 1980s and 1990s, intensive testing of lanthanoid salts (La, Ce, Nd, etc), primarily lanthanoid chlorides, were carried out as environmentally acceptable corrosion inhibitors of 7xxx series aluminum alloys [8−10]. The Ce-chloride showed the greatest protective ability.

During the occurrence of corrosion reactions in the chloride solution which contains a Ce-chloride inhibitor, there is an increase in the pH value on and near cathodic IMCs. Consequently, on the surface of those IMCs, a hardly soluble layer of Ce-hydroxide/oxide is formed [8−11]. The formed Ce-hydroxide/oxide layer significantly diminished the cathodic reaction, slowing down the entire corrosion process.

Various salts of cerium, such as Ce-perchlorates [10], Ce-nitrates [12−14], Ce-sulfates [10,12,15], Ce-diphenyl-phosphates [16], Ce-citrate [17], Ce-acetates [10,18], and Ce-cysteine [19,20] were tested recently. Inhibitor Ce-acetate showed the best protective ability. Recently, RODIČ and MILOŠEV [12,15] intensively evaluated the Ce-acetate in chloride solution as an inhibitor on different aluminum alloys, without and in the presence of Na-sulphate. They proposed the possible mechanism of the inhibitory action.

PEJIĆ et al [19] compared the corrosion protection using Ce-chloride, Cysteine, Ce-chloride + Cysteine mixture, and synthesized the Ce-cysteine complex, as corrosion inhibitors of the aluminum alloy in chloride solution. The Ce-chloride + Cysteine mixture showed the best corrosion protection, probably due to the presence of a significant synergetic effect between components of the mixture. Cerium was present in Ce(III) and Ce(IV) oxidation states in the mixture, and as a Ce(IV) oxidation state in the Ce-cysteine complex. The authors proposed and analyzed the mechanisms of inhibitory action [19].

Recently MARUNKIĆ et al [21] evaluated Ce-propionate, Ce-acetate, and Ce-formate in NaCl solution as corrosion inhibitors of aluminum alloy. The greatest protective ability was shown by the Ce-propionate inhibitor [21,22]. The Ce-propionate complex, besides the cerium cations and carboxylate anions, contains a longer aliphatic chain compared to other tested carboxylic acids.

The aim of this work is to evaluate the corrosion protection of the Ce-adipate inhibitors in a concentration that is 6 times lower than the optimal Ce-salt concentration [12]. Cerium, as well as other lanthanoids, are expensive and deficient metals, so the development of an effective corrosion inhibitor in a significantly lower concentration of cerium is of great economic importance. The adipate anion has two carboxyl groups and four carbon atoms connecting these two carboxyl groups. It can be expected that such an adipate structure enables the formation of various types of complexes with the cerium ions, as well as their binding to the aluminum alloy surface. The aliphatic chain from four carbon atoms can additionally increase the degree of water contact angle at the AA7075 aluminum alloy surface. The Zn-adipate was examined as a carbon steel corrosion inhibitor in well water [23] and obtained an inhibitory effect of ~95%. There is less data on testing of the adipate salts as corrosion inhibitors of aluminum alloys.

2 Experimental

2.1 Materials

AA7075 specimens were cut from an extruded bar with 30 mm in diameter and 7 mm in thickness. The chemical composition of AA7075 alloy was determined using X-ray fluorescence spectroscopy (XRF) (Table 1).

Table 1 Chemical composition of AA7075 alloy (wt.%)

Zn	Mg	Cu	Cr	Si
5.35	2.09	1.44	0.20	0.14
Fe	Mn	Ti	Zr	Al
0.13	0.030	0.024	0.020	Bal.

Before performing electrochemical experiments, the specimens were grounal with 1500-grit grinding paper, rinsed with bi-distilled water, and air dried. Specimens for SEM/EDS analysis were additionally polished with Al_2O_3 polishing paste (1 and 0.3 μm in grain size), and rinsed with bi-distilled water.

A WTW inoLab pH730 pH meter was used to measure the pH values of NaCl solutions and inhibitor solutions. The measured pH values are given in Table 2. A schematic view of the adipate anion is shown in Fig. 1(a), while its 3D view is

shown in Fig. 1(b). As can be seen, an adipate anion besides two carboxylate groups, contains an aliphatic chain with four carbon atoms. Sodium adipate is broadly used in many industries. It is used as a food additive, as a complexing agent, and as an acidity regulator. Also, it is used in cosmetics and personal care products, and in addition, it is used as a stabilizer of polyvinyl chloride (PVC). Sodium adipate is a colourless environmentally-friendly solid that is readily soluble in water.

Table 2 pH value of 0.5 mol NaCl + inhibitor solutions

Inhibitor	pH
–	5.7
0.75 mmol/L Na-adipate	6.6
0.5 mmol/L Ce-chloride	5.4
0.5 mmol/L Ce-adipate	5.9

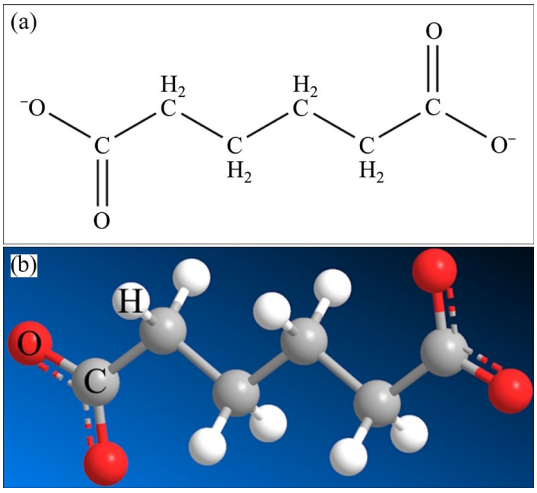

Fig. 1 (a) Schematic 2D view and (b) 3D view of adipate anion

2.2 Methods

2.2.1 Electrical conductivity

To assess the extent of the precipitation of AA7075 after one-step and two-step aging, the electrical conductivity was measured. The Foerster Sigmatest 2.069 commercial device working on the base of eddy current was applied. ASTM standard [24] gives the correlation between the electrical conductivity and resistance of AA7075 to stress corrosion cracking.

2.2.2 EIS measurements

EIS tests were carried out in a classic three-electrode electrochemical cell in NaCl solution in the presence of various inhibitors (listed in Table 2). For measurements, the electrochemical instrument potentiostat/galvanostat GAMRY 620 was used. The working electrode was the test specimen (AA7075 with surface area of 1 cm^2), the reference electrode was a saturated calomel electrode (SCE), and the counter electrode was a Pt-mesh. After establishing a relatively stable corrosion potential (up to 1 h), a sinusoidal voltage with amplitude of 10 mV and frequency from 100000 Hz to 0.01 Hz were applied to the specimens. The corresponding Nyquist and Bode (Bode-modulus and Bode-phase) plots were registered. Each experiment was carried out three times, and representative results are shown in this work.

2.2.3 LSV measurements

LSV tests were carried out in the same solutions and using the same electrochemical setup as the EIS measurements. After the formation of a relatively stable corrosion potential, φ_{corr} (up to 1 h), a potential of −0.2 V vs φ_{corr} was assigned to the working electrode (AA7075, with surface area 1 cm^2). The electrode potential is shifted to the anodic region, with a sweep rate of 0.5 mV/s. The experiment ended at the electrode potential in the anode area when a current density increased suddenly, which implicated the growth of the stable pits (pitting potential, φ_{pit}). Each experiment was carried out three times, and representative results are shown in this work.

2.2.4 Contact angle measurements

Water contact angle at the AA7075 surface was tested after 24 h of immersion in inhibitive solutions, at room temperature. A drop of bi-distilled water was put on the dried specimen surface. Images were recorded by the Smart 5MP Pro, Delta Optical microscope, and the contact angle was evaluated using the Image-Pro Plus 4.0 software.

2.2.5 SEM/EDS analysis

The appearance of the surface (as well as its composition) before and after electrochemical measurements were evaluated using a scanning electron microscope (SEM) JEOL JSM−6610LV working at 20 kV, equipped for energy dispersive spectroscopy (EDS) measurements.

2.2.6 XPS analysis

After grinding with abrasive paper of 1500 grit, specimens for XPS analysis were ultrasonically degreased, rinsed with bidistilled water, and immersed for 24 h in NaCl solution with Ce-adipate inhibitor (Table 2). XPS analysis of the AA7075 specimens was carried out by SPECS systems with an XP50M X-ray source and PHOIBOS 100/150

analyzer. The Al K_α source was used. Spectra were analyzed with the CasaXPS software package.

3 Results and discussion

3.1 Results of electrical conductivity testing

Measured values of the electrical conductivity were 30.1% and 39.3% (IACS), for one-step and two-step aged specimens, respectively.

In the process of one-step aging of AA7075, GP zones and the semicoherent η' phase with high elastic strains in solid solution are formed, which causes the dissipation of electrons during eddy current measurements, and low electrical conductivity is obtained.

The formation of stable η phase $Mg(Zn,Cu)_2$, during two-step aging of the AA7075, causes less elastic strains in solid solution and higher electrical conductivity [25,26].

3.2 Surface view of AA7075 specimens

The AA7075 microstructure is very complex. Besides the strengthening precipitates of nanometer dimensions, which are responsible for the high strength of the alloys, anodic and cathodic intermetallic particles (IMCs) of significantly larger dimensions (up to several micrometers) are present in the microstructure of the AA7075.

Anodic IMCs usually contain Mg and Si, and they are dark in SEM microphotographs (Fig. 2). In NaCl solutions, these particles to a less extent affect the corrosion characteristics of the AA7075. In the initial period of exposure to the chloride solution, their dissolution and the formation of micrometer-sized pits occur (at the place on the AA7075 surface where these particles have existed). Micrometer pits do not significantly affect the properties and macro appearance of this alloy. The EDS elementary mapping for the Mg and Si content in the annodic IMCs is shown in Figs. 2(e, f). A brighter colour means a higher concentration, while a darker colour refers to a lower concentration of appropriate elements. The presence of the brighter fields in Figs. 2(e, f) indicates a higher concentration of Mg and Si at these locations.

In addition to anodic IMCs, the AA7075 also contains cathodic IMCs with a significant amount of Cu and Fe, and they are light in colour in SEM microphotographs (Fig. 2). The corresponding EDS elementary mapping is shown in Figs. 2(c, d). Brighter fields indicate that there is a higher concentration of Cu and Fe, as constituents of the cathodic IMCs. Due to their cathodic character (much more noble electrode potential compared to surrounding Al-matrix), a cathodic reaction occurs on their surface [27−29].

Cathodic IMCs noticeably reduce the resistance of the AA7075 to corrosion. The most favorable places for the occurrence of the anodic reactions (dissolution of Al-matrix) are the edges of the cathodic IMCs. Over time, trenches are formed and then transformed into corrosion pits, or some types of intergranular corrosion (Fig. 3). Figure 3(a) shows a surface view of the AA7075 alloy, obtained by

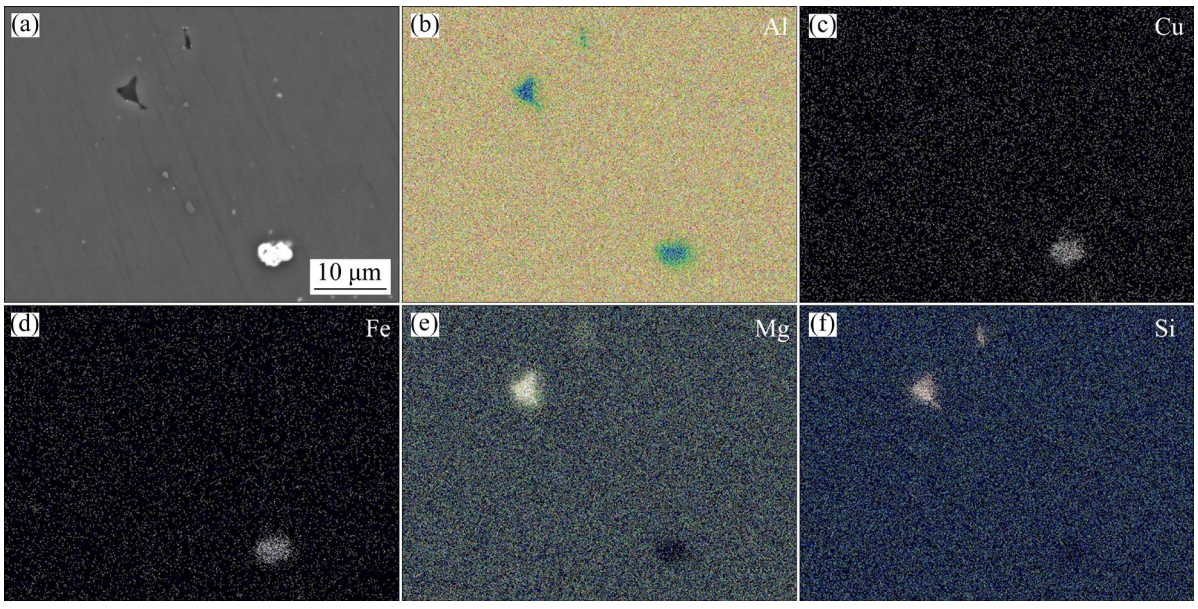

Fig. 2 SEM image and EDS elementary mappings of AA7075 alloy

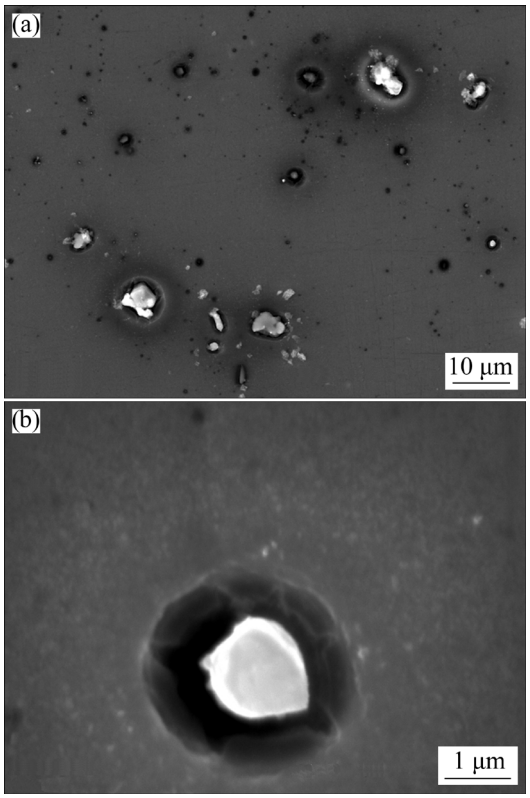

Fig. 3 Surface view of AA7075 after testing in NaCl solution with (a) lower magnification and (b) higher magnification

SEM microscopy, after testing in NaCl solution with lower magnification, while Fig. 3(b) shows a surface view at higher magnification. Trenches formed around cathodic IMCs are visible. The corrosive properties of IMCs in aluminum alloys have been analyzed previously [6,30−35]. As mentioned before, the 7xxx series aluminum alloys, after one- and two-step aging also contain fine hardening precipitates of nanometer dimensions [36−42].

3.3 Influence of chloride and adipate solutions without cerium

The polarization resistance (R_p) determined from the Nyquist diagram (Fig. 4(a)), in NaCl solution, as well as in NaCl solution containing Na-adipate inhibitor is very low. As previously discussed, in neutral chloride solutions trenches are very quickly formed around the borders of the cathodic IMCs. The formation of the trench is confirmed by the small diameter value of the semicircle on the Nyquist (EIS) diagram (Fig. 4(a)). The presence of adipate ions (without Ce) does not significantly improve the corrosion resistance of the tested AA7075.

Figure 4(b) shows the equivalent electrical circuit (EEC) used for fitting the EIS tests. The R_e is the electrolyte resistance, and CPE is the constant phase element. The CPE contains all the inhomogeneities of the tested AA7075 surface and the inhibitor layer. The same EEC was applied to EIS measurements of AA7075 alloy in inhibitive solutions (NaCl solution containing the Ce-chloride and Ce-adipate). In this case, EIS diagrams contain two time constants. One time constant corresponds to the protective inhibitory layer (capacitance and resistance of the inhibitory layer), and the other time constant corresponds to the base metal, i.e. double layer capacitance and charge-transfer resistance of the underlying base metal. However, these time constants are very close (overlapping), and fitting experimental EIS results were performed by applying simple EEC with one time constant shown in Fig. 4(b).

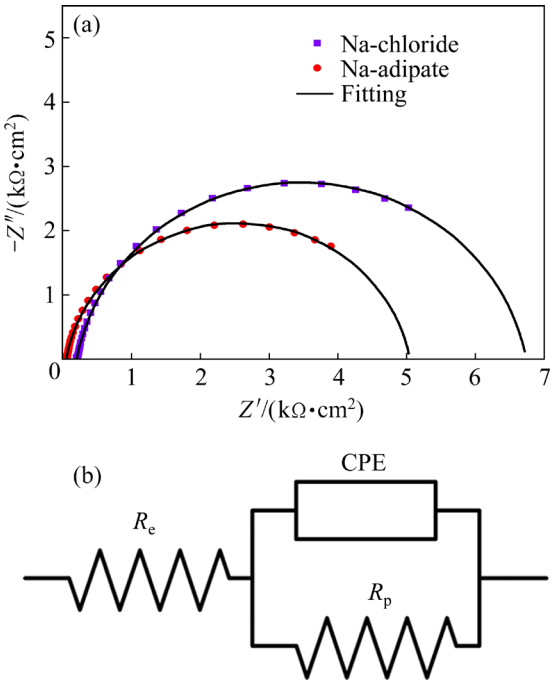

Fig. 4 (a) Nyquist diagram for AA7075 tested in Na-chloride and Na-adipate solution after 24 h and (b) electrical equivalent circuit (EEC)

Figure 5 shows the LSV diagram formed in chloride and adipate solutions (without Ce). On the LSV diagram, the cathodic and anodic branches of the polarisation curve are visible. It can be seen that both cathodic branches of the LSV curves (for pure NaCl solution and NaCl solution containing Na-adipate) practically overlap. Also, in both cases, after

reaching the corrosion potential (φ_{corr}), the value of the anodic current density starts to rise sharply. This indicates the formation of trenches around the cathodic IMCs and, consequently, the formation of corrosion pits. However, the corrosion potential formed on the surface of AA7075 alloy is higher in the case of Na-adipate solution than in the case of NaCl solution. As a consequence, the corrosion current density (J_{corr}) is slightly lower in the presence of Na-adipate (Fig. 5), which is in accordance with the polarization resistance values on the Nyquist diagram (Fig. 4(a)).

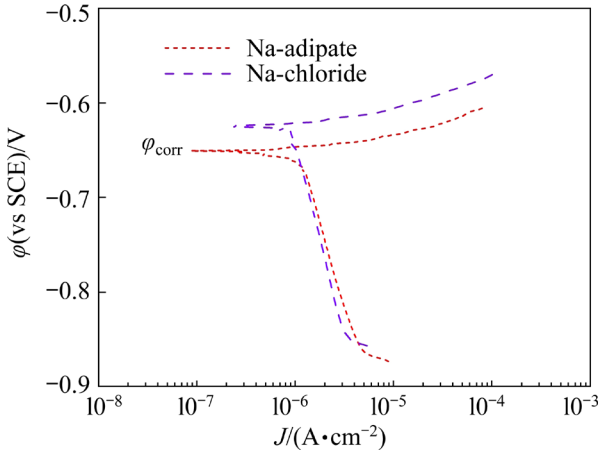

Fig. 5 LSV diagram for AA7075 tested in Na-chloride and Na-adipate solution after 24 h

Different series of aluminum alloys were previously investigated in a chloride solution [43]. In one group of aluminum alloys, the φ_{pit} was more positive than the φ_{corr}, while in another group the φ_{pit} was equal to the φ_{corr}. The AA7075 belongs to the second group of alloys.

3.4 Influence of cerium ions added in NaCl solution

The presence of cerium ions significantly increases the corrosion resistance of the AA7075. The value of R_p is about 60 times higher than that in NaCl solution without cerium (Fig. 6(a)). During the cathodic reaction (oxygen reduction reaction), there is a slight increase in the pH value of the solution on and near the cathodic IMCs. Increasing the pH value creates favorable conditions for Ce-hydroxide/oxide precipitation on the inclusion surface. The presence of Ce-hydroxide/oxide limits the occurrence of the oxygen reduction reaction and thus slows down the entire corrosion process [8−11]. Besides cathodic IMCs, Ce-hydroxide/oxide precipitates over the aluminum matrix as well, however to a lower extent, as noticed previously in the literature [44]. The solubility product constant (K_{sp}) of Ce-hydroxide is ~1.6×10^{-20} [45].

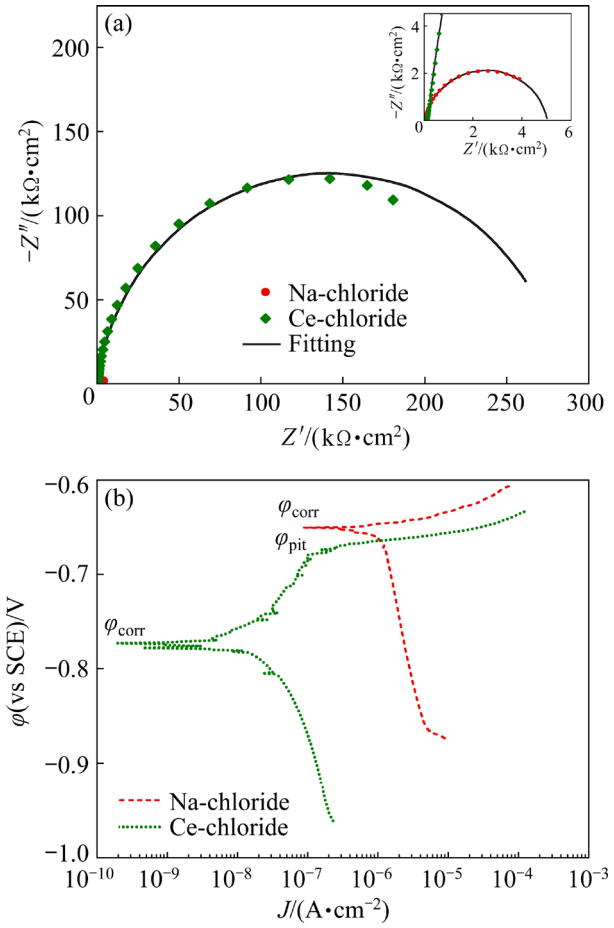

Fig. 6 (a) Nyquist diagram, and (b) LSV diagram after 24 h testing for Ce-chloride and Na-chloride solutions (Inset: Magnified initial part of the Nyquist diagram)

In the inset of the Nyquist diagram (Fig. 6(a)), the enlarged beginning part of the diagram is given. The Nyquist semicircle that corresponds to the impedance response in the NaCl solution is visible. The shape and magnitude of this Nyquist semicircle are not visible on the regular diagram without magnification.

The LSV diagram (Fig. 6(b)) contains curves for NaCl solution without and with Ce ions. As can be seen, a significantly lower current density i.e. higher corrosion resistance is obtained in a solution containing cerium ions. Much lower J_{corr} obtained in NaCl solution that contains Ce-chloride confirms this. Also, on the diagram for Ce-chloride, the φ_{corr} is transferred towards lower values of the electrode potential, and there is a relatively large pseudo-

passive area. This means that cerium chloride is an effective cathodic corrosion inhibitor and cerium chloride provides significant resistance to pitting corrosion of the AA7075.

3.5 Synergetic effect of cerium and adipate ions after 24 h testing in Na-chloride solution

The presence of Ce-adipate additionally increases the corrosion resistance of the AA7075 compared to the Ce-chloride solution (Fig. 7). The polarization resistance of AA7075 after 24 h of exposure to the solution which contains a Ce-adipate inhibitor is 740 kΩ·cm^2, and in the case of Ce-chloride, the polarization resistance is 285 kΩ·cm^2. The values of polarization resistance for NaCl and NaCl + Na-adipate are up to a hundred times lower than in inhibitory solutions that contain cerium ions. The inset in Fig. 7 shows the Nyquist diagrams for NaCl and NaCl + Na-adipate solutions (without Ce). Accordingly, inhibitive solutions, especially the solution containing Ce-adipate show a very high value of polarisation resistance (R_p). The beginning part of the diagram in Fig. 7 is given in the inset, which shows an enlarged part of the Nyquist diagram corresponding to the impedance response in the NaCl, and NaCl + Na-adipate solutions (without cerium). On the regular diagram, these Nyquist semicircles practically are not visible.

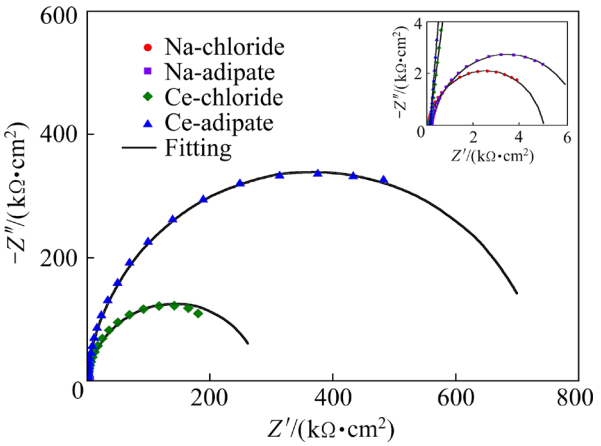

Fig. 7 Nyquist diagram for Na-chloride solution with Ce-chloride, and Ce-adipate inhibitors, after 24 h testing (Inset: Magnified initial part of the Nyquist diagram)

The synergistic effect of the Ce-chloride and Na-adipate combination is relatively high. According to the literature [46,47], the synergy effect (S) exists if $S>1$ while the synergetic effect does not exist if $S<1$. For the Ce-chloride and Na-adipate mixture, a relatively high value of synergy effect was calculated ($S\approx1.45$).

An adipate ion contains two carboxyl groups linked to an aliphatic chain of four carbon atoms. Adipate anions easily form bonds with the aluminum alloy surface and cerium ions giving various types of Ce-adipate complexes. In the beginning, in the NaCl solution which contains a Ce-adipate inhibitor, the anodic corrosion reaction is the dissolution of the matrix (AA7075) and the appropriate cathodic reaction is the reduction of oxygen (OH^- ions are released), which takes place primarily on the cathodic IMCs.

Adipate anions probably exist as a complex with cerium cations near the metal surface before their precipitation on AA7075 surface. MARKLEY et al [48] concluded that the reorganization of the cerium complexes exists near the metal surface. Similar observations can also be found in the literature [49].

Released cerium ions from the Ce-adipate complexes react with OH^- ions originating from oxygen reduction reaction, which leads to the precipitation of Ce-hydroxide/oxide on the IMCs. The mechanism of Ce-hydroxide/oxide precipitation on the surface of the cathodic intermetallic compounds was previously analyzed in detail [10,50]. The COO^- ions and mixed species with hydroxide ions bind via oxygen atoms to the AA7075 surface. A similar mechanism was previously proposed in the literature [51,52]. As a consequence, a compact inhibitory film is formed over the AA7075 surface. The presence of Ce ions, C—H and C—C bonds, and carboxylate group, were confirmed by the XPS analysis.

Results of SEM/EDS analysis (Fig. 8) show the presence of cerium on surface cathodic IMCs rich in copper and iron. As discussed above, the brighter field on the EDS elementary mappings indicates a higher amount of the tested element, while the darker field indicates a lower concentration of the appropriate elements. The presence of copper and iron in cathodic IMCs, especially Fe, is visible in Figs. 8(c, d). Also, the presence of cerium compounds on surface cathodic IMCs rich in copper and iron is visible (Fig. 8(e)). Anodic IMCs (rich in Mg) are not covered with cerium. Also, a small amount of cerium is present on the aluminum matrix surface.

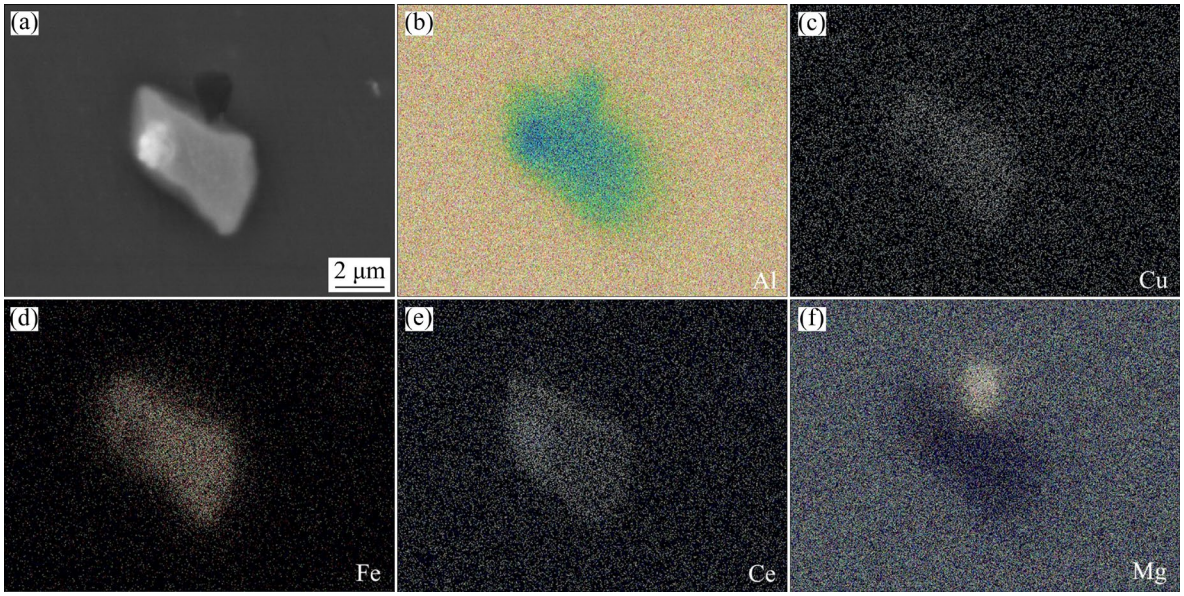

Fig. 8 SEM image and EDS surface mappings of AA7075 after 24 h testing in Ce-adipate solution

3.6 Inhibitive effect of Ce-chloride and Ce-adipate in NaCl solution during time

Bode diagrams for Ce-chloride and Ce-adipate inhibitors after a characteristic period of testing (24, 96, and 168 h) are shown in Fig. 9. The EIS results (polarisation resistance (R_p), constant phase element (CPE), and also calculated effective capacitance (C_{eff})) for all measured time are given in Table 3. The effective capacitance of the inhibitory film (C_{eff}) is determined by applying the Brug equation [53] using appropriate values for R_p, Q, and n from Table 3:

$$C_{eff}=R_p^{(1-n)/n}Q^{1/n} \quad (1)$$

During all testing time, the NaCl solution which contains a Ce-adipate inhibitor shows approximately two times higher value of polarisation resistance than the solution which contains a Ce-chloride (Table 3). Higher value of polarisation resistance in the case of Ce-adipate is the consequence of the formation of dense complexes containing bonded cerium and adipate ions. In the case of the Ce-chloride solution, Ce-hydroxide/oxide covers only cathodic IMCs, while in the case of Ce-adipate (inhibitive layer, cerium-adipate complex) it covers the AA7075 matrix.

As mentioned previously, due to overlapping, a simple equivalent electrical circuit (EEC) with one time constant was applied for fitting EIS results obtained in inhibitive solutions. As can be seen in Fig. 9 (Bode diagrams of phase angle−frequency), the time constants for the protective inhibitory layer and base metal are very close, and it is reasonable to apply this simple EEC.

The dependence of the modulus impedance $|Z|$ on frequency, both in logarithm coordinates (Bode modulus diagram) is present in Figs. 9(a−c). Values of impedance at high frequencies (10^3−10^5 Hz) correspond to electrolyte resistance. At the middle part of frequencies, curves for the Ce-adipate and Ce-chloride are linear and practically overlap. At very low frequencies (<10^{-1} Hz), these two curves are separated. The higher value of $|Z|$ at lower frequencies indicates the better protective ability of the inhibitory layer. In all diagrams (Figs. 9(a−c)), the higher value of modulus impedance at low frequencies is obtained in a solution containing Ce-adipate, than in a solution containing Ce-chloride inhibitor. The higher protective ability of Ce-adipate compared to Ce-chloride is visible in the Bode phase diagrams (Figs. 9(a−c)). Widening Bode phase diagrams at low frequencies in the case of Ce-adipate compared to Ce-chloride (and pure Na-chloride) indicate their better protective ability. Greater coverage of the metal surface and compactness of inhibitive film is probably a consequence of the widening of the characteristic phase peak. Similar behaviour (i.e. widening phase diagrams at low frequencies) in the case of other corrosion inhibitors

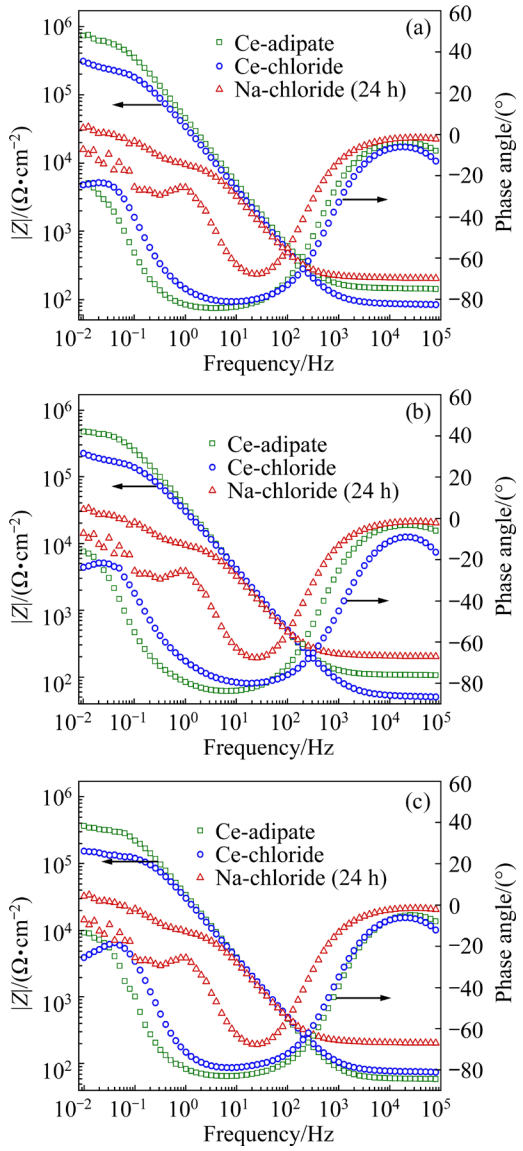

Fig. 9 Bode diagrams for Na-chloride solution containing Ce-chloride and Ce-adipate inhibitors: (a) 24 h; (b) 96 h; (c) 168 h

of aluminum alloys can be found in the literature [54]. In the Bode modulus diagram for pure NaCl solution, at middle and low frequencies, the corresponding EIS curve is shifted to lower values of modulus impedance, indicating low value of polarisation resistance. Also, compared to inhibitory solutions, a very narrow peak is obtained in the Bode phase diagram in the NaCl solution (Figs. 9(a–c)).

The time dependence of the polarisation resistance (R_p) and effective capacitance (C_{eff}) for Ce-chloride and Ce-adipate inhibitors are shown in Fig. 10. In both inhibitive solutions, the value of the polarisation resistance gradually decreases (Fig. 10(a)); however, the R_p value for Ce-adipate remains higher than for the Ce-chloride inhibitor (about two times). This is a consequence of the presence of Ce-hydroxide/oxide and appropriate complexes in the case of Ce-adipate. The shape of the diagram for Ce-adipate, i.e. the gradually decreased polarisation resistance during time, can be explained by the stability of the formed Ce-adipate complexes. During time, a gradual dissolution of the previously formed inhibitive layer occurs, and consequently its protective ability decreases. However, the value of the polarisation resistance in the case of Ce-adipate remains much higher than in the case of Ce-chloride during all measured time.

The time dependence of the effective capacitance (C_{eff}) for Ce-chloride and Ce-adipate inhibitors is shown in Fig. 10(b).

As can be expected with decreasing polarisation resistance, the value of effective capacitance (C_{eff}) generally increases (Fig. 10(b)). This regulatory is approximately correct for both inhibitors (Ce-chloride and Ce-adipate).

Table 3 Summarised results of EIS measurements

Immersion time/h	Specimen	R_e/ (kΩ·cm^2)	R_p/ (kΩ·cm^2)	CPE		C_{eff}/ (μF·cm^2)
				Q/ (μΩ^{-1}·s^n·cm^{-2})	n	
24	Ce-chloride	0.120	284	5.72	0.92	4.24
	Ce-adipate	0.145	740	3.84	0.95	4.08
48	Ce-chloride	0.060	373	5.23	0.94	5.48
	Ce-adipate	0.080	601	5.24	0.92	5.76
72	Ce-chloride	0.060	324.8	5.28	0.93	5.50
	Ce-adipate	0.195	593.8	5.48	0.92	6.05
96	Ce-chloride	0.085	265	5.41	0.92	5.59
	Ce-adipate	0.185	435	5.12	0.91	5.56
168	Ce-chloride	0.050	188	6.19	0.89	6.30
	Ce-adipate	0.165	404	5.41	0.90	5.89

3.7 Surface view after immersion in NaCl and inhibitive solutions

AA7075 specimens were held up to 240 h in inhibitive solutions to obtain direct confirmation of the protective ability of the mentioned corrosion inhibitors (Fig. 11). Already after 4 h of exposure to the NaCl solution (without inhibitor), there is a loss of metallic gloss and also a slight change in the colour of the surface. After 24 h of exposure to the NaCl solution, the colour of the specimen surface is completely changed, and surface becomes darker, with the presence of a visible layer of corrosion products. The surface degradation process continues during prolonged action of the NaCl solution (Fig. 11). Corrosion damage occurring on the surface of AA7075 alloy after 24 h of immersion in NaCl solution at high magnification, is shown in the SEM microphotographs (Figs. 3(a, b)). In these figures, trenches around cathodic IMCs, formed as a consequence of corrosion reactions on the surface of AA7075 alloy in NaCl solution, are visible. Cathodic reactions occur on surface IMCs, and anodic reaction−dissolution occurs on the surrounding aluminium matrix (around IMCs).

Surfaces of specimens immersed in solutions with Ce-chloride and Ce-adipate inhibitors show a

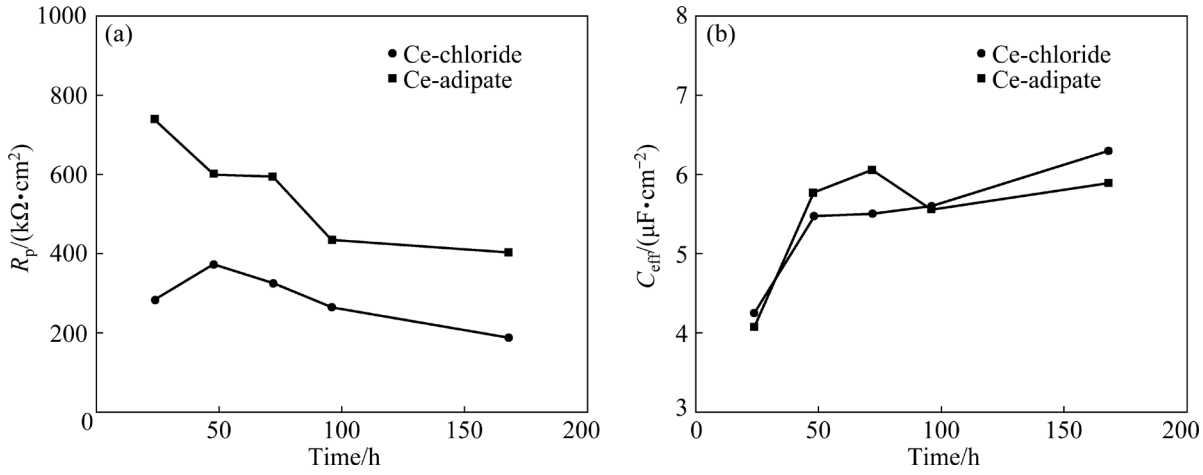

Fig. 10 Time dependence of (a) polarisation resistance (R_p) and (b) effective capacitance (C_{eff}) for Ce-chloride and Ce-adipate inhibitors

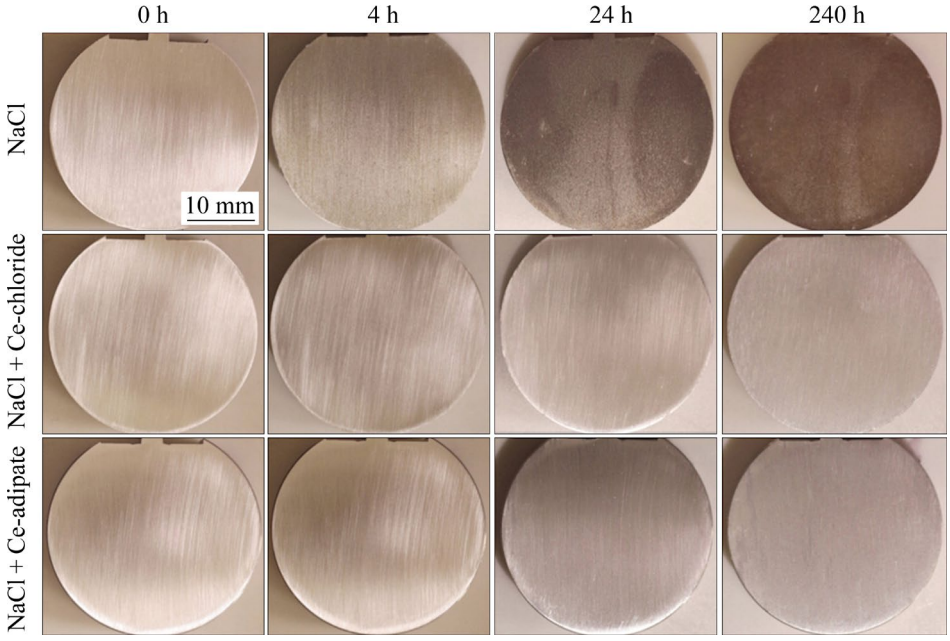

Fig. 11 Surface view of AA7075 surface immersed in Na-chloride, Ce-chloride, and Ce-adipate solution for prolonged time

slight change in brightness after 24 h. The change in brightness after 24 h action of the inhibitory solution may be attributed to the inhibitory layer formation on the surface of the specimens. The presence of Ce-oxide/hydroxide on the surface of the cathodic IMCs after 24 h held in an inhibitive solution is shown in an EDS elementary mapping (Fig. 8). A brighter field (in Ce elementary mapping) on cathodic IMCs confirms the presence of inhibitive cerium compounds. After prolonged action (up to 240 h), the process of formation of inhibitory layers was intensified.

3.8 Linear sweep voltammetry (LSV) measurements

The protective ability of the inhibitors (Ce-chloride and Ce-adipate) against corrosion of the AA7075 can also be determined based on LSV measurements. The characteristic LSV diagrams recorded after 24 and 96 h are shown in Fig. 12.

For the pure NaCl solution, after reaching the φ_{corr}, there is a sudden increase in the value of the corrosion current density. An increase in the corrosion current density shows the formation of corrosion pits. The value of the J_{corr} for pure NaCl solution has a significantly higher value than that of the NaCl solution containing inhibitors (Fig. 12). This indicates a very low resistance of AA7075 to general corrosion in the NaCl solution. This is in accordance with the results of EIS tests.

The 7075 aluminium alloy in the Ce-adipate solution has a corrosion potential that is more anodic than in the Ce-chloride solution, which is probably a consequence of the presence of the adipate ions in the solution (Fig. 12(a)). During a prolonged time, the gradual dissolution of the inhibitive complexes (probably that contains adipate ion) occurs and, consequently, the difference in corrosion potential between Ce-adipate and Ce-chloride is significantly less (Fig. 12(b)). Table 4 summarizes the results of LSV measurements. Corrosion current density values (J_{corr}) for both inhibitors, Ce-chloride and Ce-adipate, increase over time. Higher values of J_{corr} after 96 h than after 24 h indicates a lowering of the protective ability of the mentioned corrosion inhibitors. This is in accordance with the R_p value obtained by EIS measurements. In the case of Ce-adipate, during all testing periods, lower values of J_{corr} are obtained than for the Ce-chloride, which confirms its better protective abilities and these results are also in accordance with EIS measurements.

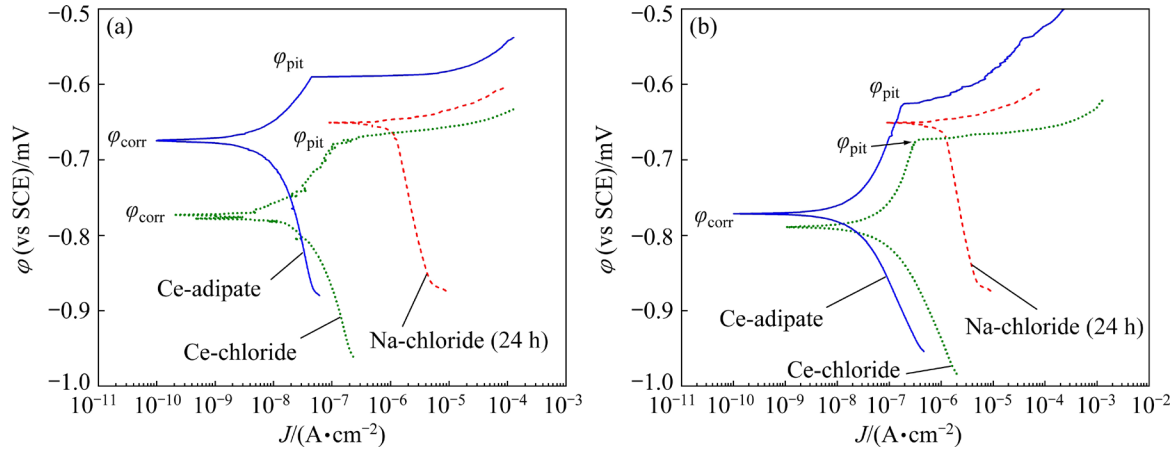

Fig. 12 LSV diagram for AA7075 after (a) 24 h and (b) 96 h testing in Na-chloride solution in presence of Ce-chloride and Ce-adipate inhibitors

Table 4 Results of LSV measurements

Immersion time/h	Specimen	φ_{corr}/mV	J_{corr}/(nA·cm^{-2})	φ_{pit}/mV	(φ_{pit}−φ_{corr})/mV
24	Ce-chloride	−775	20	−675	100
	Ce-adipate	−675	10	−590	85
96	Ce-chloride	−790	65	−670	120
	Ce-adipate	−770	20	−625	145

Contrary to pure NaCl solution, in the solution with Ce-adipate and Ce-chloride inhibitors, a relatively large pseudo-passive area is obtained. Pits appear only at potentials above the pseudo-passive region, i.e. after reaching pitting potential (φ_{pit}).

The shift of the corrosion potential to the cathodic area (in the presence of the corrosion inhibitors) compared to the pure NaCl solution indicates their cathodic character. The cathodic character of the Ce-adipate inhibitor is especially noticeable after a longer time of the inhibitory action (96 h).

3.9 Water contact angle

The results of the water contact angle measurements for Ce-chloride and Ce-adipate inhibitors are shown in Fig. 13. The higher value of contact angle for Ce-adipate solution (Fig. 13(b)) compared to Ce-chloride solution (Fig. 13(a)) also confirms its better protective ability. The aliphatic chain originating from adipate ions bonded with Ce ions in the complex on the AA7075 surface is probably the cause of the higher contact angle value, i.e. the greater protective ability of the Ce-adipate inhibitor. In the case of Ce-adipate, the contact angle is about (38.3±3.1)°, while for Ce-chloride, this value is (29.6±3.4)°.

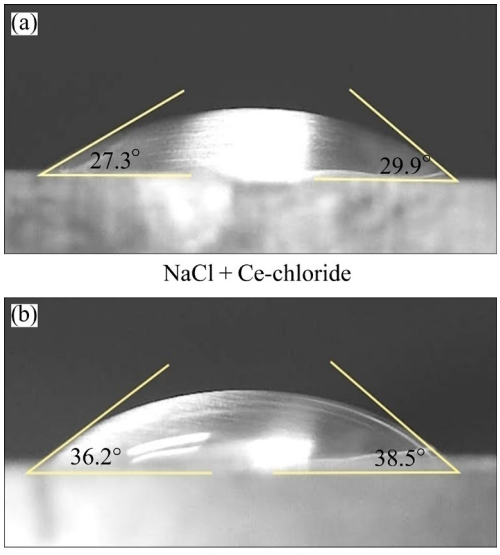

Fig. 13 Contact angle for (a) Ce-chloride and (b) Ce-adipate solution, after 24 h

3.10 XPS analysis results

The XPS survey plot in Fig. 14 shows the main peaks recorded for a specimen of AA7075 previously immersed for 24 h in a neutral NaCl solution containing the corrosion inhibitor Ce-adipate, at room temperature. The diagram was recorded in the range of binding energy from 0 to 1000 eV. The diagram shows the main peaks for Ce 3d, containing cerium in Ce(III) and Ce(IV) oxidation states, O 1s peak from Al-oxide/hydroxides, and peaks for Cl 2p and Al 2p. Also, there is the C 1s peak from carboxylate ions and C — H and C — C peaks originating from carboxylate anions.

A very similar XPS survey spectrum for AA7075 alloy previously immersed in NaCl solution with Ce-propionate was already obtained by MARUNKIĆ et al [21]. Inhibitor Ce-propionate is a cerium salt of mono-carboxylic acid, opposite to Ce-adipate which is a cerium salt of two-carboxilic acid. Inhibitor Ce-propionate contains an aliphatic chain with two C atoms, while Ce-adipate contains an aliphatic chain with four C atoms between the carboxylate groups.

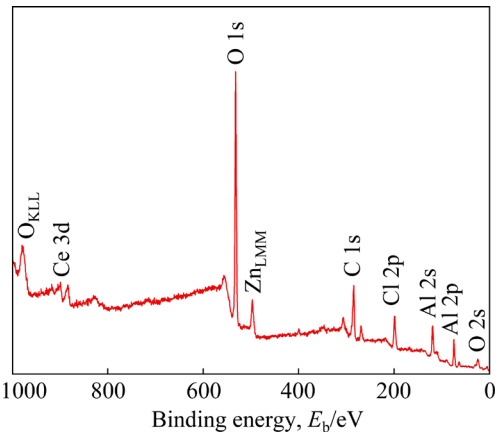

Fig. 14 XPS survey spectrum for specimens immersed in Ce-adipate solution, after 24 h

The XPS diagram for Al 2p shows the typical Al-oxides/hydroxides peak at 76.0 eV (Fig. 15(a)) and a peak at 73.7 eV corresponding to Al metal. Also, the peak for Al-oxide/hydroxide is present in the O 1s diagram (Fig. 15(b)), which contains a peak originating from cerium, as well.

The XPS diagram for Cl 2p (Fig. 15(c)) shows adsorbed chloride anions, which causes the formation of Al-chloride and other metal-chlorides that are present in the AA7075 matrix.

Figure 15(d) shows the high-resolution spectrum for Ce 3d. This spectrum contains the following three zones. The first one contains 3d peaks with a range of binding energy from 878 to

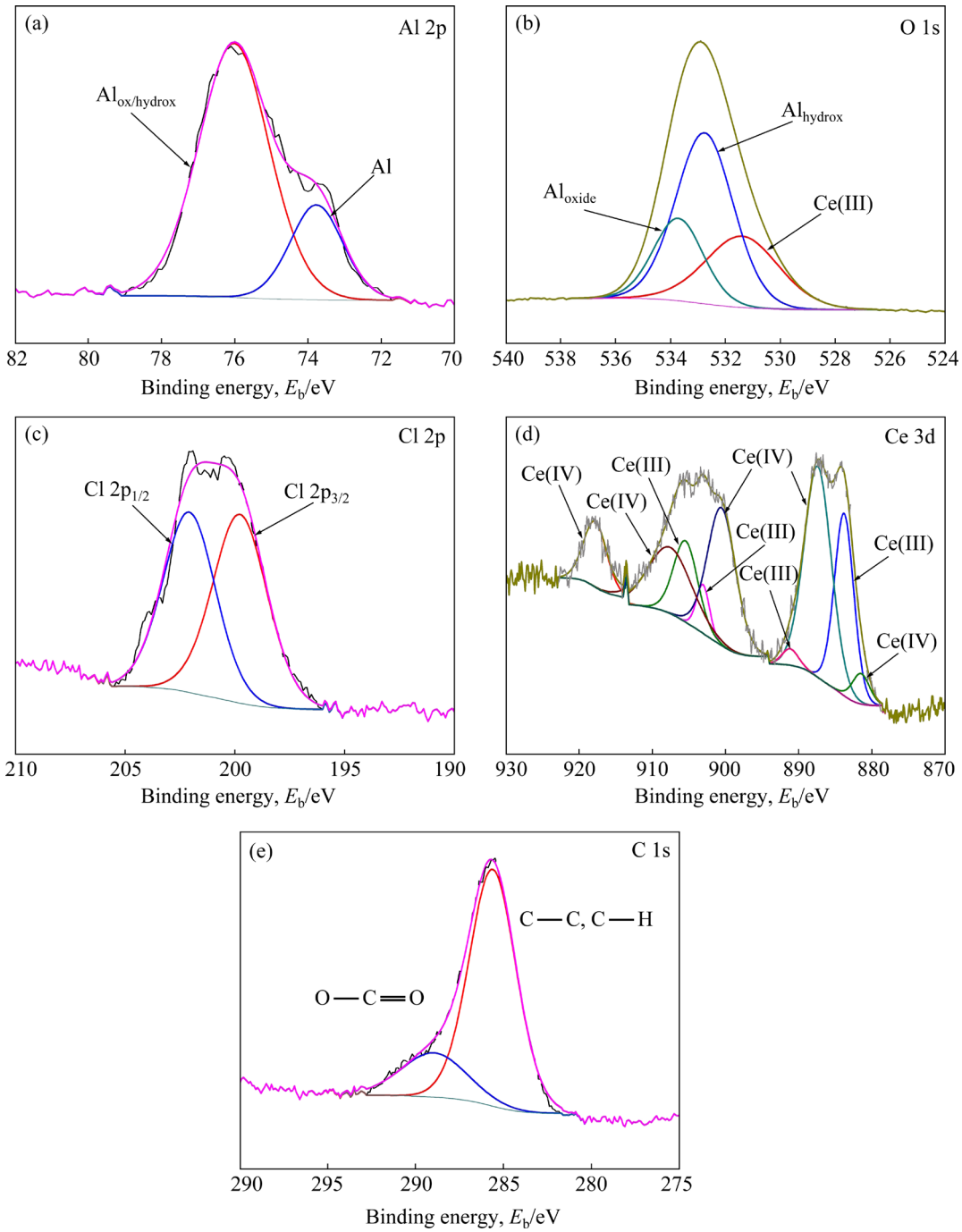

Fig. 15 High-resolution XPS spectra for different elements in inhibitive film on AA7075

892 eV, the second includes peaks with binding energy from 895 to 912 eV, and the satellite peak has a binding energy of 917.8 eV, as a third zone. Therefore, the inhibitory layer contains cerium in oxidation states (Ce(III) and Ce(IV)).

The characteristic peak for the C—H and C—C groups (285.6 eV), and the peak for the COO^- group (288.9 eV), are included in the high-resolution C 1s spectrum (Fig. 15(e)). The carboxylate groups present in the XPS spectra are a consequence of adipate $[OOC—(CH)_2—COO]^{2-}$ anions adsorption on the aluminum surface.

Recently, RODIČ et al [55] analyzed Ce-acetate as a corrosion inhibitor on the 2024 aluminium alloy in NaCl solution by applying the XPS method. Obtained values of the binding energy for appropriate compounds in high-resolution XPS spectra [55] are very close as in this work. Inhibitor Ce-acetate, similar to Ce-adipate contains cerium, a carboxylate group ($—COO^-$), and an aliphatic chain

with one C atom. Contrary to Ce-acetate, inhibitor Ce-adipate contains two carboxylate —COO^- groups and an aliphatic chain with four C atoms, between these groups.

Accordingly, the presence and composition of the formed inhibitory layer are confirmed by XPS analysis. This layer formed on the AA7075 surface, originating from the Ce-adipate inhibitor, contains cerium in the oxidation state of Ce(III) and Ce(IV). Also, Al—O bonds and different cerium complexes formed with hydroxide and adipate anions are present. This implicates the formation of Ce-adipate complexes and bonds of carboxylate ions with the aluminum surface.

4 Conclusions

(1) Ce-chloride shows a relatively good protective ability. The precipitation of the Ce-oxide/hydroxide on the cathodic IMCs diminishes the rate of corrosion.

(2) In the Ce-adipate solution, a higher value of polarization resistance (about two times), and a much lower value of corrosion current density are obtained than for the Ce-chloride solution.

(3) Both inhibitors (Ce-chloride and Ce-adipate) are good pitting corrosion inhibitors and belong to the group of cathodic inhibitors. However, somewhat higher pitting corrosion resistance is obtained in the case of the Ce-adipate than in the Ce-chloride solution, especially after a prolonged period of testing.

(4) As confirmed by XPS spectra, the inhibitive layer contains Ce in Ce(III) and Ce(IV) oxidation states and also carboxylate —COO^- groups and C—H and C—C bonds, originating from the Ce-adipate inhibitory layer.

(5) The corrosion protection of the tested inhibitors increases in a similar way as the water contact angle. The Na-chloride solution which contains the Ce-adipate inhibitor has a higher contact angle and higher inhibitory action than the Na-chloride solution which contains the Ce-chloride inhibitor.

CRediT authorship contribution statement

Jovanka N. PEJIĆ: Investigation, Writing − Original draft, Data curation; **Dunja D. MARUNKIĆ:** Conceptualization, Investigation, Writing − Original draft, Data curation; **Bojana M. RADOJKOVIĆ:** Writing − Review & editing; **Bore V. JEGDIĆ:** Conceptualization, Supervision, Writing − Review & editing, Validation; **Sanja G. ERAKOVIĆ PANTOVIĆ:** Formal analysis, Methodology, Visualization; **Anđela R. SIMOVIĆ:** Formal analysis, Visualization; **Behar ALIĆ:** Resources, Validation; **Milica GVOZDENOVIĆ:** Validation, Supervision, Project administration.

Declaration of competing interest

The authors declare that they have no known competing financial interests or personal relationships that could have appeared to influence the work reported in this paper.

Acknowledgments

This study was financially supported by the Ministry of Science, Technological Development and Innovation of the Republic of Serbia (Nos. 451-03-66/2024-03/200026, 451-03-65/2024-03/200135).

References

[1] HATCH J. Aluminum properties and physical metallurgy [M]. Ohio: ASM International, Metal Parks, 1984.

[2] DAVIS J. Corrosion of aluminum and aluminum alloys [M]. Ohio: ASM International, Metal Parks, 1999.

[3] VARGEL C. Corrosion of aluminium [M]. 2nd ed. Amsterdam: Elsevier, 2020.

[4] BUCHHEIT R. A compilation of corrosion potentials reported for intermetallic phases in aluminum alloys [J]. Journal of The Electrochemical Society, 1995, 142: 3994−3996. https://doi.org/10.1149/1.2048447

[5] BIRBILIS N, CAVANAUGH M, BUCHHEIT R. Electrochemical behavior and localized corrosion associated with Al7Cu2Fe particles in aluminum alloy 7075-T651 [J]. Corrosion Science, 2006, 48: 4202−4215. https://doi.org/10.1016/j.corsci.2006.02.007

[6] BIRBILIS N, BUCHHEIT R. Electrochemical characteristics of intermetallic phases in aluminum alloys-an experimental survey and discussion [J]. Journal of The Electrochemical Society, 2005, 152: B140−B151. https://doi.org/10.1149/1.1869984

[7] PELLERIN C, BOOKER S. Reflections on hexavalent chromium: Health hazards of an industrial heavyweight [J]. Environmental Health Perspectives, 2000, 108: A402−A407. https://www.ncbi.nlm.nih.gov/pmc/articles/PMC2556938/pdf/ehp0108-a00402.pdf

[8] ARNOTT D, HINTON B, RYAN N E. Cationic-film-forming inhibitors for the protection of the AA 7075 aluminum alloy against corrosion in aqueous chloride solution [J]. Corrosion, 1989, 45: 12−18. https://doi.org/10.5006/1.3577880

[9] ARNOTT D, RYAN N E, HINTON B, SEXTON B, HUGHES

A. Auger and XPS studies of cerium corrosion inhibition on 7075 aluminum alloy [J]. Applications of Surface Science, 1985, 22/23: 236−251. https://doi.org/10.1016/0378-5963(85)90056-X

[10] HINTON B. Corrosion inhibition with rare earth metal salts [J]. Journal of Alloys and Compounds, 1992, 180: 15−25. https://doi.org/10.1016/0925-8388(92)90359-H

[11] DEYAB M A, ABD EL-REHIM S S A, HASSAN H, SHALTOT A. Impact of rare earth compounds on corrosion of aluminum alloy (AA6061) in the marine water environment [J]. Journal of Alloys and Compounds, 2020, 820: 153428. https://doi.org/10.1016/j.jallcom.2019.153428

[12] RODIČ P, MILOŠEV I. Corrosion inhibition of pure aluminium and alloys AA2024-T3 and AA7075-T6 by cerium(III) and cerium(IV) salts [J]. Journal of The Electrochemical Society, 2016, 163: C85−C93. https://doi.org/10.1149/2.0431603jes

[13] MANSFELD F. Use of rare earth metal salt solutions for corrosion protection of aluminum alloys and mild steel [J]. Russian Journal of Electrochemistry, 2000, 36: 1063−1071. https://doi.org/10.1007/BF02757525

[14] VOLARIČ B, MILOŠEV I. Rare earth chloride and nitrate salts as individual and mixed inhibitors for aluminium alloy 7075-T6 in chloride solution [J]. Corrosion Engineering, Science and Technology, 2017, 52: 201−211. https://doi.org/10.1080/1478422X.2016.1245957

[15] RODIČ P, MILOŠEV I. The influence of additional salts on corrosion inhibition by cerium(III) acetate in the protection of AA7075-T6 in chloride solution [J]. Corrosion Science, 2019, 149: 108−122. https://doi.org/10.1016/j.corsci.2018.10.021

[16] HILL J A, MARKLEY T, FORSYTH M, HOWLETT P, HINTON B. Corrosion inhibition of 7000 series aluminium alloys with cerium diphenyl phosphate [J]. Journal of Alloys and Compounds, 2011, 509: 1683−1690. https://doi.org/10.1016/j.jallcom.2010.09.151

[17] MARUNKIĆ D, PEJIĆ J, JEGDIĆ B, MARINKOVIĆ A, RADOJKOVIĆ B. Cerium citrate as ecologically friendly corrosion inhibitor for AA7075 alloy mater [J]. Materials and Corrosion, 2022, 73: 950−960. https://doi.org/10.1002/maco.202112900

[18] MILOŠEV I, RODIČ P. Cerium chloride and acetate salts as corrosion inhibitors for aluminum alloy AA7075-T6 in sodium chloride solution [J]. Corrosion, 2016, 72: 1021−1034. https://doi.org/10.5006/1956

[19] PEJIĆ J, JEGDIĆ B, RADOJKOVIĆ B, MARUNKIĆ D, MARINKOVIĆ A, BAJAT J. Cysteine and cerium as green corrosion inhibitors for AA7049: Mixture vs. complexation [J]. Corrosion Science, 2022, 209: 110815. https://doi.org/10.1016/j.corsci.2022.110815

[20] PEJIĆ J, RADOJKOVIĆ B, MARUNKIĆ D, JEGDIĆ B, STEVANOVIĆ S, MILOŠEVIĆ M, BAJAT J. Inhibitory effect of cysteine and lanthanides on AA7075-T6 in neutral NaCl solution [J]. Materials and Corrosion, 2022; 73: 1800−1812. https://doi.org/10.1002/maco.202213330

[21] MARUNKIĆ D, PEJIĆ J, JEGDIĆ B, LINIĆ S, PERIŠIĆ J, RADOJKOVIĆ B, MARINKOVIĆ A. Inhibitory effect of cerium salts of lower carboxylic acids on Al−Zn−Mg−Cu alloy in NaCl solution [J]. Journal of The Electrochemical Society, 2021, 168: 081501. https://doi.org/10.1149/1945-7111/ac1895

[22] RADOJKOVIĆ B, MARUNKIĆ D, MILOŠEVIĆ M, GRUBIŠIĆ S, PEJIĆ J, JEGDIĆ B, MARINKOVIĆ A. Analysis of the Ce(III) chloride, Ce(III) nitrate, and Ce(III) propionate as corrosion inhibitor of the aluminum alloys in NaCl solution [J]. Materials and Corrosion, 2022, 73: 1604−1614. https://doi.org/10.1002/maco.202213177

[23] FLORENCE R H, ANTHONY N, SAHAYARAJ W, AMALRAJ J, RAJENDRAN S. Corrosion inhibition of carbon steel by adipic acid – Zn^{2+} system [J]. Indian Journal of Chemical Technology, 2005, 12: 472−476.

[24] ASTM B 221M-13. Standard specification for aluminum and aluminum - alloy extruded bars, rods, wire, profiles, and tubes [S]. West Conshohocken, Pennsylvania, United States: ASTM International (ASTM).

[25] AZARNIYA A, TAHERI A K, TAHERI K K. Recent advances in ageing of 7xxx series aluminum alloys: A physical metallurgy perspective [J]. Journal of Alloys and Compounds, 2019, 781: 945−983. https://doi.org/10.1016/j.jallcom.2018.11.286

[26] NOVIKOV I I. Theory of heat treatment of metals [M]. Moscow: Mir Publishers, 1978.

[27] ANDREATTA F, LOHRENGEL M, TERRYN H, de WIT JHW. Electrochemical characterisation of aluminium AA7075-T6 and solution heat treated AA7075 using a micro-capillary cell [J]. Electrochimica Acta, 2003, 48: 3239−3247. https://doi.org/10.1016/S0013-4686(03)00379-7

[28] ANDREATTA F, TERRYN H, de WIT J H W. Effect of solution heat treatment on galvanic coupling between intermetallics and matrix in AA7075-T6 [J]. Corrosion Science, 2003, 45: 1733−1746. https://doi.org/10.1016/S0010-938X(03)00004-0

[29] ANDREATTA F, TERRYN H, de WIT J H W. Corrosion behaviour of different tempers of AA7075 aluminium alloy [J]. Electrochimica Acta, 2004, 49: 2851−2862. https://doi.org/10.1016/j.electacta.2004.01.046

[30] SUN Yuan-wei, PAN Qing-lin, SUN Yu-qiao, WANG Wei-yi, HUANG Zhi-qi, WANG Xiang-dong, HUB Quan. Localized corrosion behavior associated with Al7Cu2Fe intermetallic in Al−Zn−Mg−Cu−Zr alloy [J]. Journal of Alloys and Compounds, 2019, 783: 329−340. https://doi.org/10.1016/j.jallcom.2018.12.151

[31] BUCHHEIT R, BIRBILIS N. Electrochemical microscopy: An approach for understanding localized corrosion in microstructurally complex metallic alloys [J]. Electrochimica Acta, 2010, 55: 7853−7859. https://doi.org/10.1016/j.electacta.2010.04.046

[32] BIRBILIS N, BUCHHEIT R. Investigation and discussion of characteristics for intermetallic phases common to aluminum alloys as a function of solution pH [J]. Journal of The Electrochemical Society, 2008, 155: C117−C126. https://doi.org/10.1149/1.2829897

[33] ZHU Ya-kun, SUN Kai, FRANKEL G. Intermetallic phases in

aluminum alloys and their roles in localized corrosion [J]. Journal of The Electrochemical Society, 2018, 165: C807−C820. https://doi.org/10.1149/2.0931811jes

[34] CAVANAUGH M, LI Ji-chao, BIRBILIS N, BUCHHEIT R. Electrochemical characterization of intermetallic phases common to aluminum alloys as a function of solution temperature [J]. Journal of The Electrochemical Society, 2014, 161: C535−C543. https://doi.org/10.1149/2.0361412jes

[35] JI Yuan-yuan, XU Yun-ze, ZHANG Bin-bin, BEHNAMIAN Y, XIA Da-hai, HU Wen-bin. Review of micro-scale and atomic-scale corrosion mechanisms of second phases in aluminum alloys [J]. Transactions of Nonferrous Metals Society of China, 2021, 31: 3205−3227. https://doi.org/10.1016/S1003-6326(21)65727-8

[36] GUO Yue, ZHANG Jian-hai, ZHAO Hong-wei. Microstructure evolution and mechanical responses of Al−Zn−Mg−Cu alloys during hot deformation process [J]. Journal of Materials Science, 2021, 56: 13429−13478. https://doi.org/10.1007/s10853-021-06095-7

[37] YUAN Ding-ling, CHEN Song-yi, CHEN Kang-hua, HUANG Lan-ping, CHANG Jiang-yu, ZHOU Liang, DING Yun-feng. Correlations among stress corrosion cracking, grain-boundary microchemistry, and Zn content in high Zn-containing Al−Zn−Mg−Cu alloys [J]. Transactions of Nonferrous Metals Society of China, 2021, 31: 2220−2231. https://doi.org/10.1016/S1003-6326(21)65650-9

[38] FANG Xu, SONG Min, LI Kai, DU Yong, ZHAO Dong-dong, JIANG Chao, ZHANG Hong. Effects of Cu and Al on the crystal structure and composition of $\eta(MgZn_2)$ phase in over-aged Al−Zn−Mg−Cu alloys [J]. Journal of Materials Science, 2012, 47: 5419−5427. https://doi.org/10.1007/s10853-012-6428-9

[39] GOSWAMI R, LYNCH S, HOLROYD H, KNIGHT S, HOLTZ R. Evolution of grain boundary precipitates in Al 7075 upon aging and correlation with stress corrosion cracking behavior [J]. Metallurgical and Materials Transactions A, 2013, 44: 1268−1278. https://doi.org/10.1007/s11661-012-1413-0

[40] MA Zhi-min, ZHANG Yong, LIU Sheng-dan, DENG Yun-lai, ZHANG Xin-ming. Quenching sensitivity and heterogeneous precipitation behavior of AA7136 alloy [J]. Transactions of Nonferrous Metals Society of China, 2021, 31: 3356−3369. https://doi.org/10.1016/S1003-6326(21)65734-5

[41] LI X M, STARINK M. Effect of compositional variations on characteristics of coarse intermetallic particles in overaged 7000 aluminium alloys [J]. Materials Science and Technology, 2001, 17: 1324−1328. https://doi.org/10.1179/026708301101509449

[42] LIU Fang, ZHENG Jing-xu, CHEN Xia, XU Xue-song, CHEN Bin. Study on corrosion resistance of artificially aged 7075 aluminium alloy by using Cs-corrected STEM [J]. Transactions of Nonferrous Metals Society of China, 2022, 32: 2828−2837. https://doi.org/10.1016/S1003-6326(22)65986-7

[43] MCCAFFERTY E. Introduction to corrosion science [M]. New York: Springer, 2010.

[44] PAUSSA L, ANDREATTA F, de FELICIS D, BEMPORAD E, FEDRIZZI L. Investigation of AA2024-T3 surfaces modified by cerium compounds: A localized approach [J]. Corrosion Science, 2014, 78: 215−222. https://doi.org/10.1016/j.corsci.2013.10.001

[45] SPEIGHT J. Lange's handbook of chemistry [M]. New York: McGraw-Hill, 2017.

[46] MURAKAWA T, NAGAURA S, HACKERMAN N. Coverage of iron surface by organic compounds and anions in acid solutions[J]. Corrosion Science, 1967, 7: 79−89. https://doi.org/10.1016/S0010-938X(67)80105-7

[47] POPOOLA L T. Organic green corrosion inhibitors (OGCIs): A critical review [J]. Corrosion Reviews, 2019, 37: 71−102. https://doi.org/10.1515/corrrev-2018-0058

[48] MARKLEY T, FORSYTH M, HUGHES A E. Corrosion protection of AA2024-T3 using rare earth diphenyl phosphates [J]. Electrochimica Acta, 2007, 52: 4024−4031. https://doi.org/10.1016/j.electacta.2006.11.028

[49] KOKALJ A. Molecular modeling of organic corrosion inhibitors: Calculations, pitfalls, and conceptualization of molecule–surface bonding [J]. Corrosion Science, 2021, 193: 109650. https://doi.org/10.1016/j.corsci.2021.109650

[50] BETHENCOURT-NÚÑEZ M, BOTANA F J, CALVINO J J, MARCOS M, RODRIGUEZ-CHACON M A. Lanthanide compounds as environmentally-friendly corrosion inhibitors of aluminium alloys: A review [J]. Corrosion Science, 1998, 40: 1803−1819. https://doi.org/10.1016/S0010-938X(98)00077-8

[51] BLIN F, KOUTSOUKOS P G, KLEPETSIANIS P, FORSYTH M. The corrosion inhibition mechanism of new rare earth cinnamate compounds−Electrochemical studies [J]. Electrochimica Acta, 2007, 52: 6212−6220. https://doi.org/10.1016/j.electacta.2007.04.001

[52] FORSYTH M, SETER M, HINTON B, DEACON G, JUNK P. New 'green' corrosion inhibitors based on rare earth compounds [J]. Australian Journal of Chemistry, 2011, 64: 812−819. https://doi.org/10.1071/CH11092

[53] HIRSCHORN B, ORAZEM M, TRIBOLLET B, VIVIER V, FRATEUR I, MUSIANI M. Constant-phase-element behavior caused by resistivity distributions in films: II. Applications [J]. Journal of The Electrochemical Society, 2010, 157: C458−C463. https://doi.org/10.1149/1.3499565

[54] ECCO L G, ROSSI S, DEFLORIAN F, FEDEL M. Electrochemical behavior of AA5005 aluminum alloy in acidic chloride-based medium containing CeO_2 nanoparticles [J]. Journal of The Electrochemical Society, 2018, 165: C933−C938. https://doi.org/10.1149/2.0371814jes

[55] RODIČ P, LEKKA M, ANDREATTA F, MILOŠEV I, FEDRIZZI L. The synergistic effect of cerium acetate and sodium sulphate on corrosion inhibition of AA2024-T3 at various temperatures [J]. Electrochimica Acta, 2021, 370: 137664. https://doi.org/10.1016/j.electacta.2020.137664.

己二酸铈作为 AA7075 铝合金的绿色缓蚀剂

Jovanka N. PEJIĆ[1], Dunja D. MARUNKIĆ[1], Bojana M. RADOJKOVIĆ[1], Bore V. JEGDIĆ[1], Sanja G. ERAKOVIĆ PANTOVIĆ[1], Anđela R. SIMOVIĆ[1], Behar ALIĆ[2], Milica GVOZDENOVIĆ[3]

1. Institute of Chemistry, Technology, and Metallurgy, University of Belgrade, Njegoševa 12, Belgrade, Serbia;
2. Metallurgical Institute “Kemal Kapetanović”, Travnička cesta 7, 72000 Zenica, Bosnia and Herzegovina;
3. Faculty for Technology and Metallurgy, University of Belgrade, Karnegijeva 4, Belgrade, Serbia

摘　要：对比研究了基于己二酸铈和氯化铈的低浓度绿色缓蚀剂对 7075 铝合金在中性 NaCl 电解质中腐蚀的影响。采用电化学阻抗谱和线性扫描伏安法研究腐蚀行为，采用扫描电子显微镜和 X 射线光电子能谱(XPS)对合金浸入腐蚀介质后的表面进行研究。电化学实验表明，己二酸铈比氯化铈具有更高的极化电阻值(约 2 倍)和更低的腐蚀电流密度，因此具有更好的腐蚀抑制效果。这两种缓蚀剂都具有阴极缓蚀剂的作用，具有较强的抗点蚀能力，并且在腐蚀介质中长时间浸泡(240 h)时能够提供足够的保护。XPS 分析表明，使用己二酸铈缓蚀剂的样品表面缓释膜中 Ce 以 Ce(III)和 Ce(IV)的氧化态形式存在，且存在羧酸—COO^-、C—C 和 C—H，这些均与防腐效率的提高有关。

关键词：AA7075；绿色缓蚀剂；己二酸铈

(Edited by Bing YANG)